Experimental and numerical study of needle peening effects on Aluminum alloy 2024-T3 sheets

Hongyan Miao [a], Julio Méndez [a], Sylvain Forgues [b], Martin Lévesque [a]
[a] CREPEC, Département de Génie Mécanique, École Polytechnique de Montréal, Canada,
hong-yan.miao@polymtl.ca, martin.levesque@polymtl.ca;
[b] Shockform Aéronautique Inc., Canada, sylvain.forgues@shockform.com

Keywords: Needle peening, finite element modeling, peen forming

Introduction

Shockform Aeronautique Inc. is a Quebec based pioneer in peening equipment solutions for repairs of high-value components in the aerospace and defense industries. Shockform is currently developing a portable needle peening tool called the SPIKER® for peen forming and local repairs. These developments aim to establish needle peening as a viable alternative to manual shot peening and rotary flapper peening for niche applications. Needle peening uses relatively hard spikes, called needles, powered by a pneumatic source in order to hit the surface of a ductile workpiece. As the powered tool is pressed against and moved along the component's surface, the impacting needles stretch the impacted surface, creating indentations as seen in Figure 1(a). The bulk of the substrate surrounding the deformed material opposes this stretching, therefore creating a region of compressive stresses, as seen in Figure 1(b). The near-surface compressive layer of the deformed material hinders crack propagation under cyclic loading and therefore increases the material's fatigue life.

Needle peening results in a clean procedure that does not require media collection systems. This process is suitable for manufacturing environments where Foreign Object Damage (FOD) and personnel health and safety would be compromised by using a non-captive peening technology. The absence of consumable material also makes it optimal for local repairs and constitutes therefore a highly practical portable repair equipment. Needle peening has a high adoption potential because of its portable design and operational features that target niche overhaul needs currently not covered by current peening equipment.

Objectives

The first objective of this work was to characterize the operation of the needle peening equipment, and to understand the relationship between the peening velocity and the frequency of the impacts as a function of air pressure. The second objective was to experimentally measure residual stresses induced by the process applied on AA2024 and develop numerical models for their prediction.

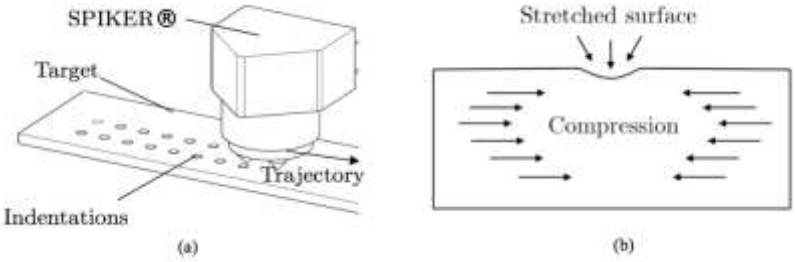

Figure 1 Generation of indentations by needle peening. (a) Creation of indentations due to needle Impacts; (b) Development of a compression area as a response to the indentation.

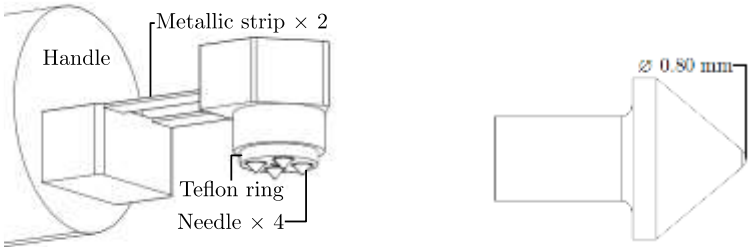

Figure 2 Simplified representation of the needle peening equipment prototype. (a) SPIKER® head components; (b) side-view of a first generation needle tip.

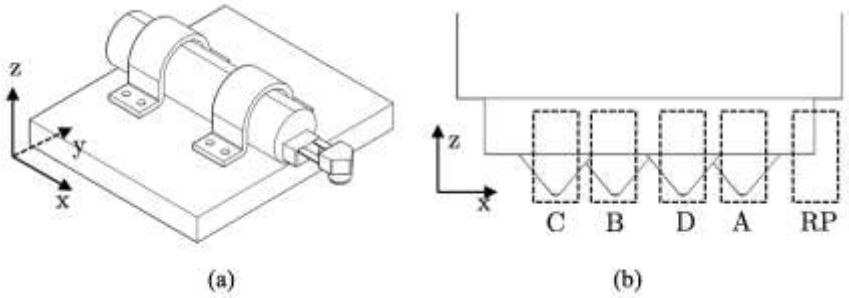

Figure 3 High-speed camera recording set-up with needles A, B, C and D edge of tool reference point RP

Methodology

Equipment

The equipment used for the study was a prototype portable pneumatic needle peening equipment as shown in Figure 2(a). The air powered handheld device featured four protruding needles traveling along their axes due to the pneumatic pressure and internal mechanisms. The needle tip geometry is shown in Figure 3(b). The needle tip was attached to a needle sleeve to form a full needle. The head was covered by a teflon ring that controlled the stand-off distance during peening.

High speed photography was used to analyze the dynamics of the needles during peening under various operation conditions. The tool was held into place by means of two steel straps, as seen in Figure 3(a). A high-speed recording camera MotionBlitz® Cube4 was used with a 60 mm *f*2.8 lens perpendicular to the X-Z plane. The tool head was rotated slightly to have the four needles in frame simultaneously, as shown in Figure 3(b).

The operation parameters were selected using the tooling's internal digital controller for air pressure p=10, 15, 20, 25, and 30 psi (0.068, 0.1, 0.14, 0.17 and 0.2MPa). The frames were recorded individually as .bmp files at a recording frequency of 5000 fps at a resolution of 480 ×206 pp. For each of the operating pressures, the recording lasted 200 ms, meaning that 1000 frames were obtained per pressure. The time step between frames was 200 μs. In total, 5000 images were obtained. MATLAB was used to analyse the collection of images obtained from the high-speed camera recording. A subroutine divided each frame into sub-frames to analyse each needle individually, as well as the edge of the tool head which served as a reference point RP, as shown in Figure 3. The needles were labelled as needle A, needle B, needle C and needle D, and the edge of the tool as RP. The positions of each needle tip at different times were recorded, as shown in Figure 4, and used to calculate the velocity of each needle at different pressures.

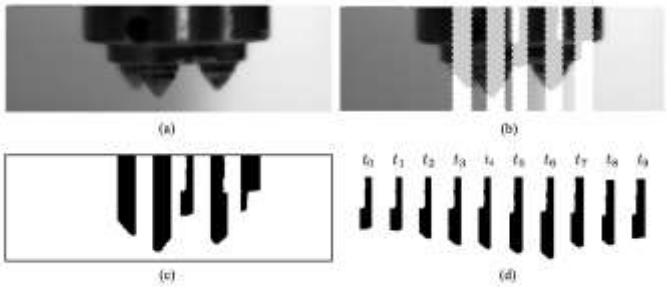

Figure 4 Image processing of the needle peening with p=20 psi (0.14 MPa) at $t = t_0$. (a) as seen by camera, (b) sub-frame division, (c) colour shreshold, (d) Spike D at different time intervals.

Experimental procedures

Aluminum strips were peened to study the material response in terms of intensity at a given set of peening parameters. The measured arc heights were then compared with predictions from numerical models. As only one needle geometry was selected for this study, the sole varying parameter was the air pressure with p= 10, 15, 20, 25, and 30 psi (0.068, 0.1, 0.14, 0.17 and 0.2MPa). AA2024-T3 aluminum sheets of 1.6 mm thickness were cut into test specimens with dimensions similar to those of a standardized Almen strip according to SAE J442 [1]. Six (6) samples were obtained for each pressure p for a total of 30 samples. The incremental treatment times chosen to develop the arc heights were t =30, 60, 120, 240 and 480 s. The deflections of strip were measured using a Coordinate Measuring Machine (CMM) during the saturation tests. Measurements were obtained in the samples' longitudinal and the transverse directions for 69.96 mm and 16.95 mm for the specimen's length and width, respectively, along its center line. The XRD technique was employed to measure the residual stress profile corresponding to pressure p=20 psi (0.14 MPa) at saturation at PROTO Manufacturing in Ontario.

Numerical analysis

FE analysis software ANSYS was used in combination with MATLAB to simulate the shot peening and peen forming processes [2]. The program allowed for generating a parametric FE model featuring the mesh, number of impacts, material properties, boundary conditions, and contact parameters. Reduced integration solid elements SOLID164 were chosen to model the target material. All properties of AA2024 were obtained from Gariépy et al. [3]. The needle material properties obeyed those of carbon tungsten. The needles were represented as half-spheres to reduce the model size. The material properties used in the model a Young's Modulus E_n =643 GPa, density ρ_n =15630 kg/m^3, and Poisson's ratio ν_n = 0.21 [4]. The needle tip radius R_n= 0.4 mm was selected based on the prototype's drawings as shown in Figure 2. The needles were approximated as rigid hemispheres meshed with SHELL163. The needle impacted on the surface randomly. The needle velocity obtained from high speed camera and image analysis was input as an initial boundary condition. The induced stresses obtained from the dynamic impact model represent the material in an unbalanced state. The FE model developed by Gariépy et al. [3]was used to predict the specimen deflection at the center by defining the residual stresses as initial boundary conditions. The calculated deflections at different peening times were used to obtain the saturation curve and to calculate the saturation point.

Results and analysis

The average impact velocity for a needle A, B, C, D per pressure p obtained from the high-speed characterization is presented in Figure 5. It is observed that the relationship between the velocity at impact and the air pressure is almost linear. This trend was expected since increasing the air pressure provides more energy to activate the needles. The impact velocity of needle A is the most sensitive to the increase of air pressure. Needles B and C show similar response to the change in air pressure in a lower extent than needles A and D.

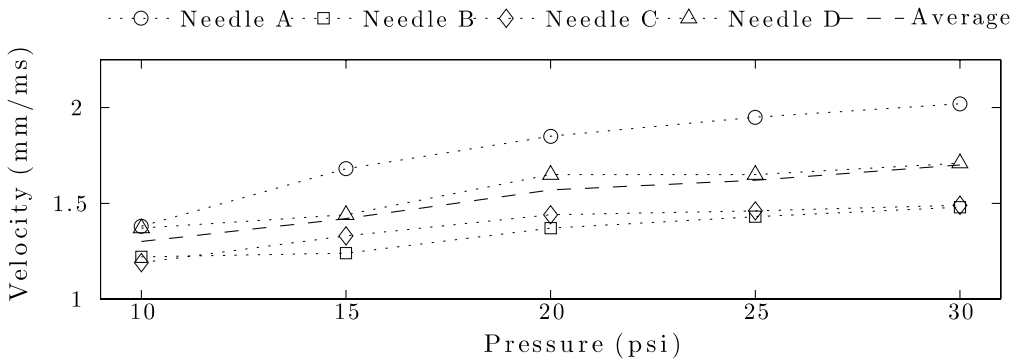

Figure 5 Individual needle velocities as a function of air pressure

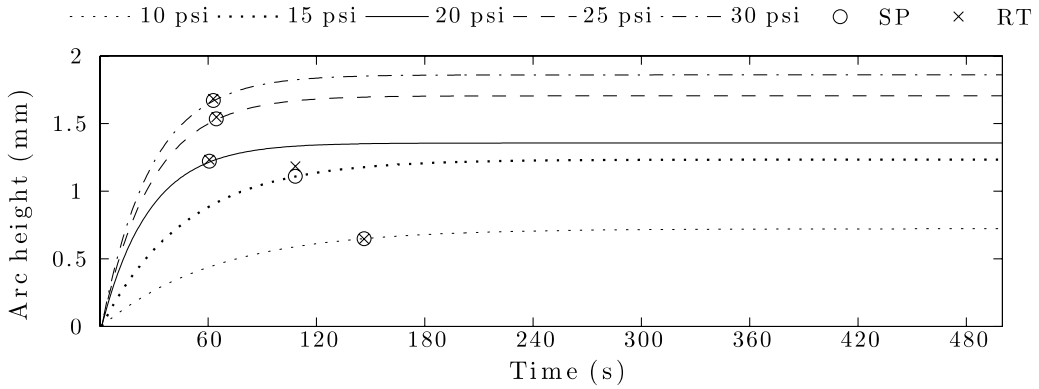

Figure 6 Arc height curves for p = {10, 15, 20, 25, 30} psi using CMM values. SP means simulated saturation point.

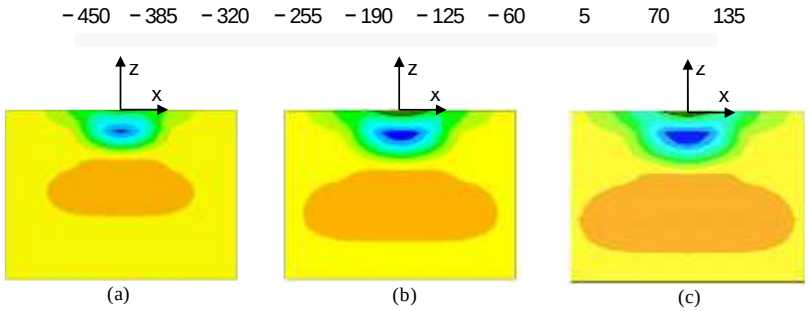

Figure 7 Cross-section induced stresses (MPa) contour plot after single impact for (a) v= 1.30 mm/ms, (b) *v* = 1.57 mm/ms and (c) *v* = 1.70 mm/ms

Figure 6 shows the arc height curves for *p*= 10, 15, 20, 25, 30 psi (0.068, 0.1, 0.14, 0.17 and 0.2MPa) from the CMM measurements. The arc height increased with the increase of pressure values. The re-test (RT) arc height measurements were provided for reference only. The deflection values obtained at the simulated saturation points can be used as a reference in order to assess the adequacy of the prediction of needle peening results by means of numerical methods.

Figure 7 shows the cross-sections (X = [-0.4, 0.4], Y=0 and Z = [0, -0.6]) of the impact point (centered on X=Y=0) and the surrounding material for *v*= 1.30, 1.57, 1.70 mm/ms from one shot peening simulation. The scaling factor of plots was set to 2 in the post-processing result viewer for a better appreciation of the surface deformation. The same contour plot value limits were established for the three cases. The plastic deformation difference at the impact point between the three scenarios is

obvious. The diameter of the indentation increased with the increase of v. It is observed that the penetration depth shows the same incremental trend in relation to v. The maximum compressive stress is found underneath the surface aligned with the impact point and its print increases for higher energy impacts. The compressive and the tensile stresses introduced by the impact increased in magnitude and extension as v increased, with a difference in the maximum compressive stress of 5% between v = 1.30 mm/ms and v = 1.70 mm/ms.

Figure 8 shows the average induced stress profiles calculated with a 1.6 mm thick impact model for N = {10, 20, 40, 80, 160, 320} randomly located impacts for a velocity v = 1.57 mm/ms, which corresponds to a pressure of 20psi. The stress profiles were obtained by averaging the nodal solution of stress σ_x of the nodes in the representative region as a function of the depth z. It can be seen that the depth of compressive residual stresses increased with the number of impacts. In addition, the surface stress magnitude, the maximum compressive stress in the near-surface and the maximum tensile stress deeper in the material increased with the increase of N. The depth at which the maximum compressive stress was found did not increase significantly, being located at around 0.08mm inside the target. It can also be seen that as N approached its greatest value, the degree of change in the stress profile is less noticeable, which suggests that the material converged towards saturation.

Figure 9 shows the simulated arc height generated with the FE forming model using the predicted average induced stresses as input. Given that the impact locations were generated randomly, it was suspected that the average induced stresses would be influenced by the impact distribution. In order to account for the stochastic nature of the simulation, five repetitions were run for each value of N with different impact coordinates. The simulated saturation was found to occur at N=137 impacts with a resulting specimen deflection of Ah_{sat}=1.24 mm. Therefore the model developed predicted that the studied sample reached its saturation point after N=137 impacts, according to the definition of Almen intensity.

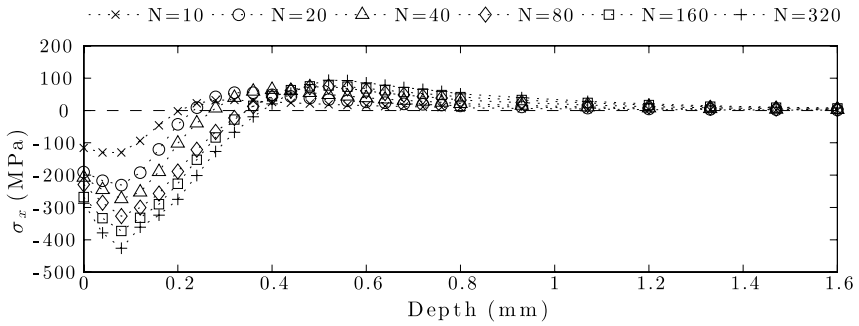

Figure 8 Average induced stress from FE simulation: N = {10, 20, 40, 80, 160, 320}, v = 1.57 mm/ms.

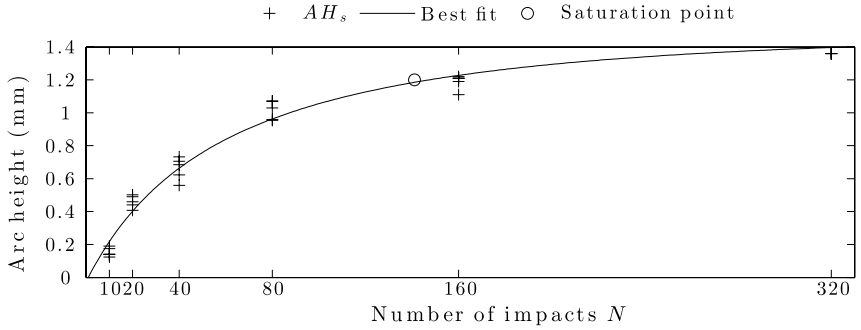

Figure 9 Simulated arc heights and fitted saturation curve for v = 1.57 mm/ms.

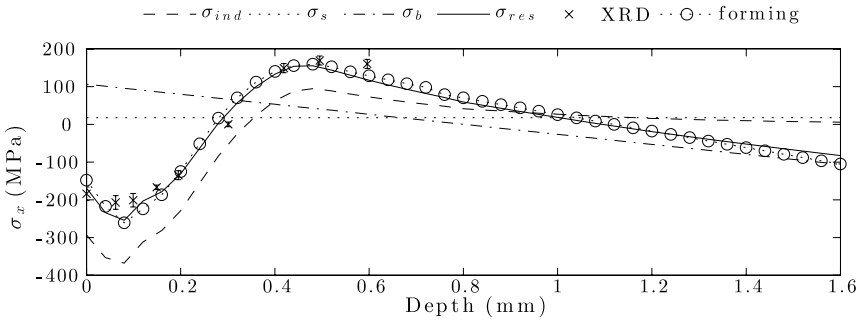

Figure 10 Residual stress balancing for saturation of v = 1.57 mm/ms and comparison with experimental results. σ_{ind} is induced stress, σ_s is stretching stress, σ_b is bending stress, and σ_{res} is residuals stress [5].

Figure 10 shows the comparison between the balanced residual stress profile predicted after N=137 impacts at v = 1.57 mm/ms using the random multiple impact model and the residual stresses determined experimentally by the XRD method. Overall, there is good accordance between the predicted and experimental results. The surface residual stress and the tensile stress in the material are accurately predicted. Additionally, the residual stress profile obtained as a result of the material deflection from the peen forming model is compared against the solution of the balanced stress profile obtained from the induced stresses. Both profiles are in close resemblance to the experimental results.

Conclusions

The methodology proposed in this research sets a robust combination of experimental and numerical techniques leveraged to assess the performance and predict the results of needle peening. The principal conclusions of this study are:

1) The needle peening tool, the SPIKER®, is capable of being characterized by a combination of high-speed photography and numerical algorithms that allow a detailed study of the equipment's dynamics at different operating pressures.
2) A dynamic random impact model that utilizes the dynamic properties of the peening equipment can be used to predict the induced stresses by needle peening AA2024-T3 sheets.
3) The residual stresses predictions were validated by experimental measurements.
4) The predicted induced stresses can be used as input data of existing forming models to predict the material deflection of Almen-sized AA2024-T3 strips.

Reference

1. SAEJ442, *Test strip, holder, and gage for shot peening.* 2013.
2. Miao, H.Y., Larose, S., Perron, C., and Lévesque, M., *On the potential applications of a 3D random finite element model for the simulation of shot peening.* Advances in Engineering Software, 2009. **40**: p. 1023-1038.
3. Gariépy, A., Larose, S., Perron, C., and Lévesque, M., *Shot peening and peen forming finite element modelling – Towards a quantitative method.* International Journal of Solids and Structures, 2011. **48**(20): p. 2859-2877.
4. Cardarelli, F., *Materials Handbook: A Concise Desktop Reference.* Springer, 2008.
5. Guagliano, M., *Relating Almen intensity to residual stresses induced by shot peening: A numerical approach.* Journal of Materials Processing Technology, 2001. **110**: p. 277-286.